THE ASTRONOMICAL JOURNAL, 118:1461–1467, 1999 October

OPTICAL AND NEAR-INFRARED SPECTROSCOPY OF CYGNUS A

ROBERT J. THORNTON, JR., AND ALAN STOCKTON
Institute for Astronomy, University of Hawaii, 2680 Woodlawn Drive, Honolulu, HI 96822

AND

SUSAN E. RIDGWAY
Department of Physics and Astronomy, Johns Hopkins University, Homewood Campus, Baltimore, MD 21218
Received 1999 February 22; accepted 1999 June 10

ABSTRACT

We present optical and near-infrared spectroscopy of the luminous radio galaxy Cygnus A (3C 405). Optical ($\sim$6700–9300 Å) observations were obtained of the central region, including the region where most emission lines are strongest, about 1.″5 northwest of the nucleus. However, high-ionization lines ([Ar XI] and [Fe XI]), as well as an unidentified feature at $\sim$7608 Å, are stronger in the continuum-dominated southeast component. We detect the near-infrared Ca triplet in absorption, and we use it to obtain a new determination of the redshift and velocity dispersion of the stellar component of Cygnus A. The infrared ($\sim$1.9–2.5 μm) spectrum of the nucleus shows emission from [Si VI], [S XI], and possibly [Si XI]. A number of molecular hydrogen transitions were also detected; their ratios favor X-ray heating from the nuclear source over other possible origins (e.g., shocks) as the most likely excitation mechanism. We see no evidence for broad-line wings on the Paα line profile, confirming that the broad-line region in Cygnus A remains heavily obscured at 2 μm.

Key words: galaxies: active — galaxies: individual (Cygnus A) — infrared radiation

1. INTRODUCTION

According to the unified model for radio galaxies and quasars (e.g., Barthel 1989), a Faranoff-Riley II (FR II) source is classified as a quasar when we view the object close to the axis of the obscuring torus, allowing us to see the nucleus directly; otherwise, we would call it a radio galaxy. Cygnus A provides an excellent opportunity to test this hypothesis. It is by far the most powerful radio galaxy at low redshift, for at $z \approx 0.056$ it has the radio power of typical 3C radio galaxies at redshift $z \sim 1$. The presence of high-ionization lines in its optical spectrum suggests that Cyg A harbors an active nucleus. The most direct way to confirm the presence of a quasar nucleus is to find evidence for an obscured broad-line region (BLR).

The first concrete demonstration that Cyg A had a BLR was the discovery of broad (FWHM $\approx$ 7500 km s^{-1}) Mg II emission in the ultraviolet by Antonucci, Hurt, & Kinney (1994). More recently, Ogle et al. (1997, hereafter O97) reported broad Hα in polarized flux from the eastern, western, and nuclear components (these regions are indicated in Fig. 1). These discoveries are compelling evidence for scattered light from a hidden BLR. In addition, Djorgovski et al. (1991) claimed detection of an unresolved IR source in K and L'. Based on their extinction estimates, they suggest that the intrinsic IR luminosity is in the quasar range, and hence evidence for a quasar nucleus. If it were true that a quasar nucleus dominates the flux at $\sim$2 μm, it should be possible to detect the BLR *directly* in the Paα line.

The first comprehensive infrared spectroscopic study of Cygnus A was by Ward et al. (1991, hereafter W91), using a seven-element array detector. They detected hydrogen recombination lines, molecular hydrogen lines, and [Si VI] at λ1.9629 μm, but found no evidence for a broad component to Paα. However, the [Si VI] detection was the first for a radio galaxy and reinforced the case for the presence of a hard UV continuum. W91 also attempted to estimate the extinction toward the nucleus and determine the mechanism for the molecular hydrogen excitation, but uncertainties in line fluxes led to inconclusive results for the latter. Stockton & Ridgway (1996) gave a report on an early phase of the IR portion of our current investigation, though with independent data obtained with an older, smaller detector in CGS4 on the United Kingdom Infrared Telescope (UKIRT).

This paper presents new optical and infrared spectroscopy of Cygnus A. One of the original motivations for the optical spectroscopy was to look for the Ca II triplet ($\lambda \sim$ 8500 Å) in absorption, which often can be a very useful tool for studying stellar kinematics in nearby galaxies (Pritchet 1978; Dressler 1984). We used the triplet to attempt to obtain a better systemic velocity for the stellar component, which is difficult to detect at short wavelengths because of strong dilution by featureless continuum components. Our other main result from the optical spectrum is the identification of species present in the southeast continuum-dominated region and the northwest emission peak. From our infrared spectrum, we have identified several new features, analyzed the excitation of the molecular hydrogen lines, and searched once again for evidence for a broad-line region using the hydrogen recombination lines. We also briefly discuss the importance of coronal features such as [Si VI] and [S XI].

2. OBSERVATIONS

Optical spectra ($\lambda \sim$ 6700–9300 Å) were obtained with the Low Resolution Imaging Spectrograph (Oke et al. 1995) on the Keck I Telescope, using the 600 groove mm^{-1} grating blazed at 7500 Å and a 1.″1 slit at P.A. = $-42.^\circ2$. The three 20 minute exposures were bias-subtracted and flat-fielded, using flat-field frames from exposures of an internal halogen lamp illuminating a screen on the closed spectrograph cover. An average airglow spectrum was produced from the dithered object frames. This average was subtracted from each of the individual frames after a slight

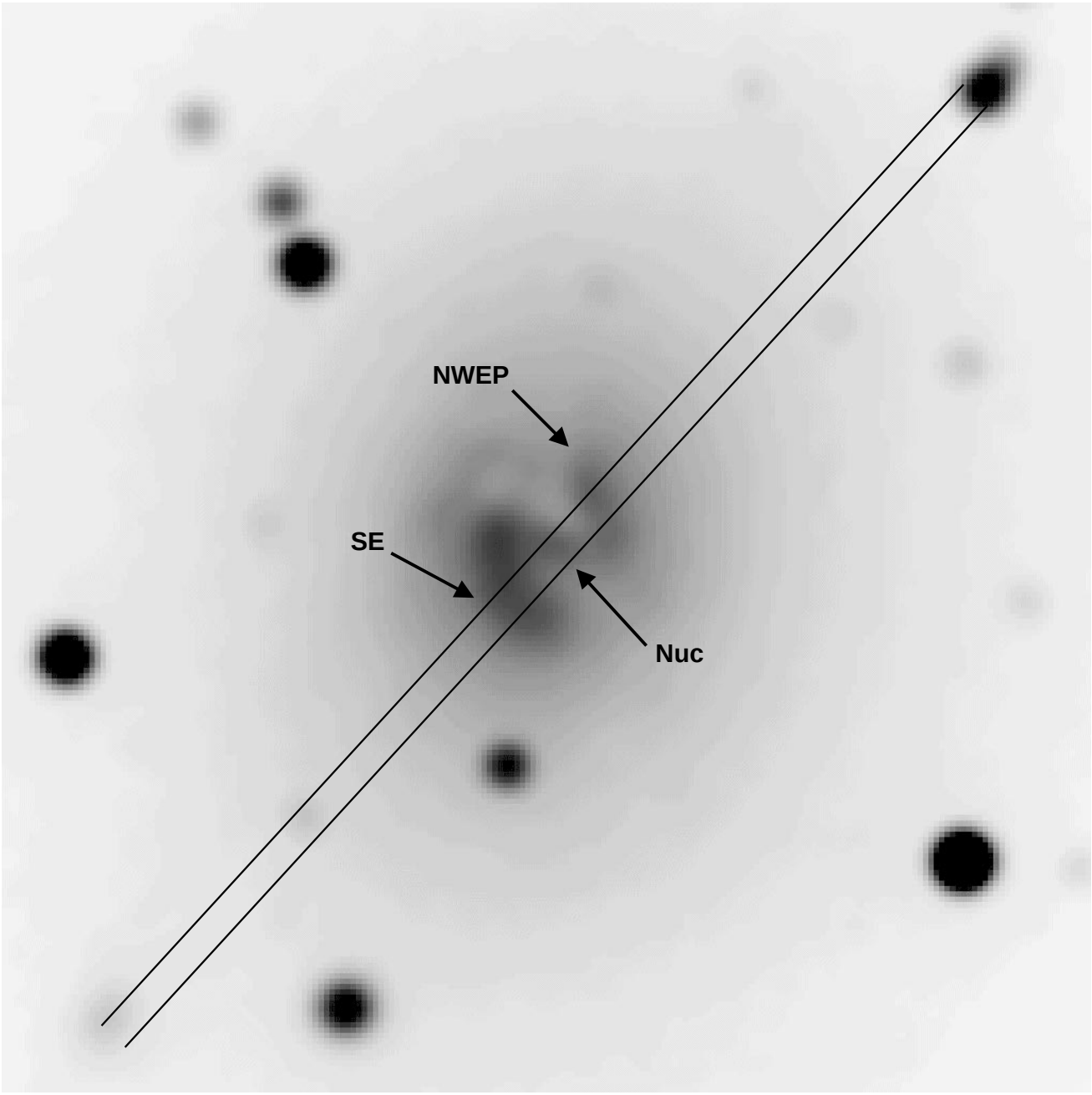

FIG. 1.—*R*-band image of the central regions of Cygnus A, showing the slit alignment for the optical spectra. North is up and east is to the right. The region shown is 22″ × 22″.

scaling and shift determined from a few prominent, unblended lines. Slight residuals remaining from this procedure were removed using the IRAF BACKGROUND task, with a linear fit to the columns perpendicular to the dispersion. The two-dimensional spectra were rectified in the dispersion coordinate by determining the mapping of a neon calibration spectrum to a coordinate system in which the lines were straight and normal to the dispersion direction and the wavelength scale was linear. The wavelength zero point was corrected for a small offset determined from prominent airglow features. The spatial coordinate was corrected for tilt and curvature of the spectrum by using IRAF tasks in the APEXTRACT package to sample the spectrum with an array of contiguous 1 pixel–wide apertures following a function fit to the continuum. The flux density of the spectrum was calibrated from an observation of the spectrophotometric standard star Wolf 1346.

IR spectra were obtained from CGS4 on the UKIRT using the 1.″2 slit, the 75 groove mm^{-1} grating, and the 150 mm camera. During the observations, the 256 × 256 InSb detector was moved parallel to the dispersion axis to oversample the spectral resolution. There were eight array positions over two pixels, so that each $\frac{1}{4}$ pixel on the actual array corresponded to 1 pixel of the output frame. The fluxes of prominent OH emission lines were used to scale and subtract the sky background in each quad-slide (object a-b-b-a dithering pattern). Line-tilt corrections were performed using standard IRAF tasks FITCOORDS and

TRANSFORM. The atmospheric transmission curve was determined by observing the B2.5 subgiant star BS 7298 before and after each object integration. The average of these two transmission measurements was then divided into the intervening Cyg A spectrum. Flux calibration was based on observations of the IR standard star HD 162208.

3. RESULTS

3.1. *Optical Emission Lines*

Figure 1 illustrates the central regions of Cygnus A and the manner in which the slit covers the northwest emission peak, the nucleus, and the southeast continuum region. The two-dimensional spectrum is shown in Figure 2, and the one-dimensional summed spectra of the northwest emission peak and the southeast continuum region are shown in Figure 3. Table 1 lists the wavelengths and fluxes of the features identified in the combined spectrum. Many of the features have been previously detected (e.g., Tadhunter, Metz, & Robinson 1994; O97), but new detections include [Ar XI] λ6917, [Ni II] λ7376, [Cl II] λ8576, and [Fe II] λ8617. There is still at least one definite new feature for which we have been unable to suggest a satisfactory identification; it appears only in the southeast peak and has a rest wavelength of ~7608 Å. The rest wavelengths for identifica-

TABLE 1

OPTICAL EMISSION FEATURES

λ Observed (Å)	λ Rest (Å)	Species	F(NW EP) ergs cm^{-2} s^{-1}	F(SE) ergs cm^{-2} s^{-1}
6797.00.....	6435.11	[Ar V]	1.44E−17	6.16E−18
6914.83.....	6548.09	[N II]	2.00E−15	8.71E−16
6930.54.....	6562.90	Hα	3.50E−15	1.58E−15
6952.31.....	6583.36	[N II]	5.98E−15	2.72E−15
7053.43.....	6678.16	He I	4.04E−17	1.10E−17
7093.65.....	6716.52	[S II]	1.66E−15	7.88E−16
7108.67.....	6730.74	[S II]	1.48E−15	6.59E−16
7299.04.....	6917:	[Ar XI]	...	5.80E−18
7399.04.....	7005.67	[Ar V]	3.71E−17	1.09E−17
7462.03.....	7065.31	He I	2.40E−17	8.80E−18
7536.45.....	7135.78	[Ar III]	3.49E−16	1.10E−16
7730.93.....	7319.92	[O II]	1.03E−16	2.87E−17
7741.78.....	7330.19	[O II]	8.73E−17	2.39E−17
7789.70.....	7378:	[Ni II]	2.32E−17	7.72E−18
8031.42.....	7605	?	...	1.31E−17
8186.26.....	7751.04	[Ar III]	8.76E−17	2.33E−17
8331.80.....	7892:	[Fe XI]	...	1.06E−17
9057.94.....	8579:	[Cl II]	3.18E−17	1.81E−17
9100.42.....	8617:	[Fe II]	1.56E−17	5.00E−18

NOTE.—Several identifications made using Tokunaga 1999.

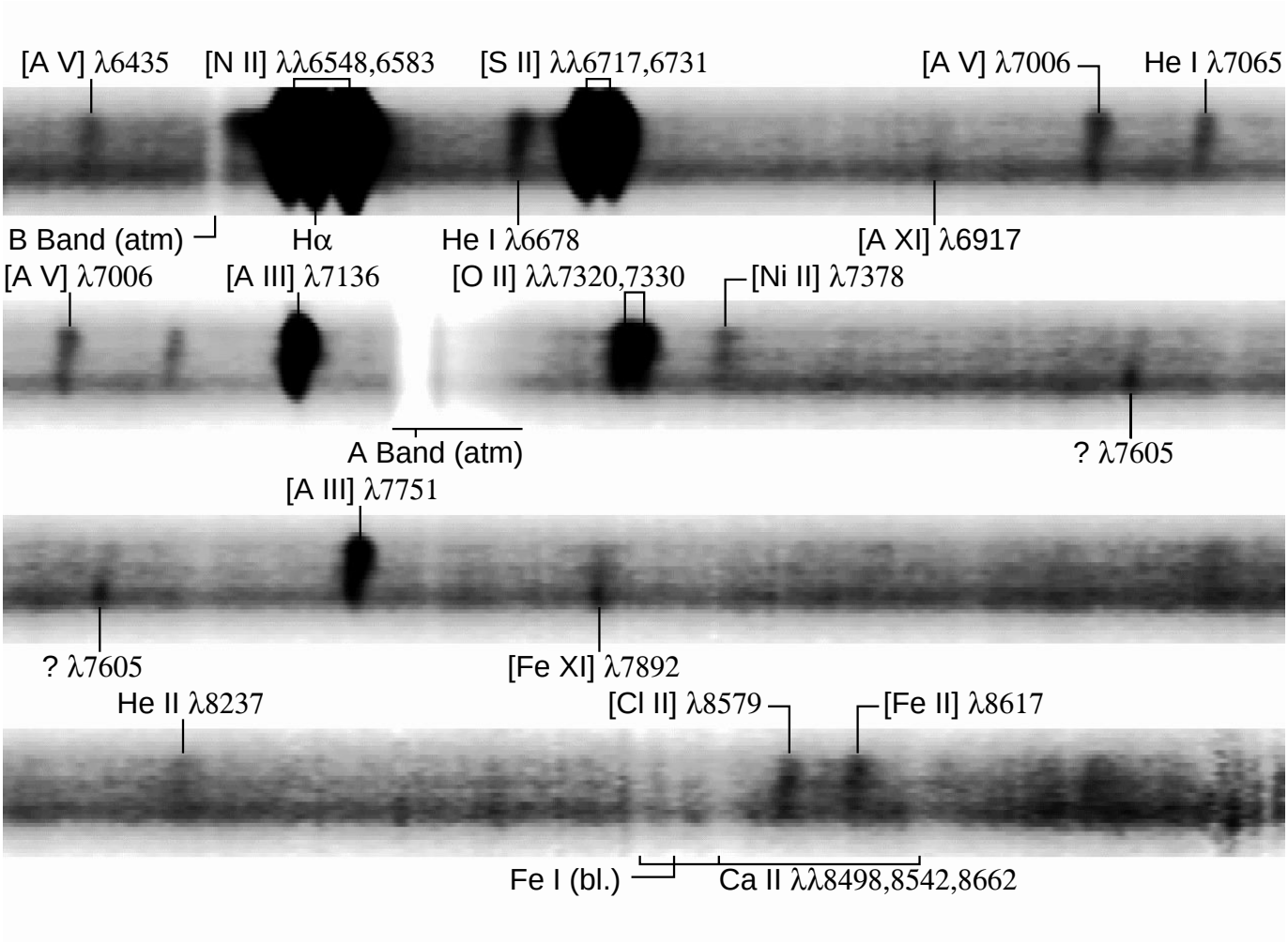

FIG. 2.—Two-dimensional optical spectrum of Cyg A. The primary regions from bottom to top along the slit are the continuum-dominated southeast region, the nucleus, and the northwest emission peak. Most of the features are most prominent in the northwest emission peak, although several are detected only in the southeast peak.

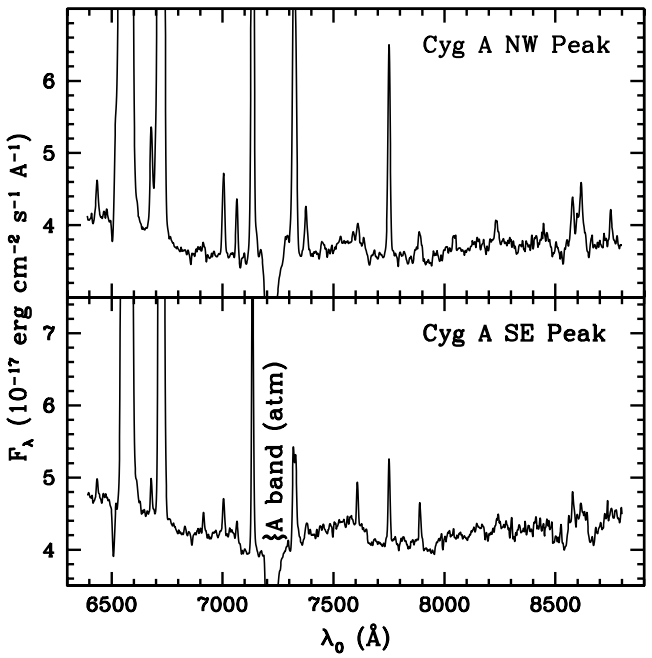

FIG. 3.—Plots of summed spectra for the northwest emission peak (*top*) and the southeast peak (*bottom*). In each case, the spectra were summed over a slit length of 0.″86 centered on the respective peaks and were then corrected to the rest frame with the appropriate emission-line redshifts.

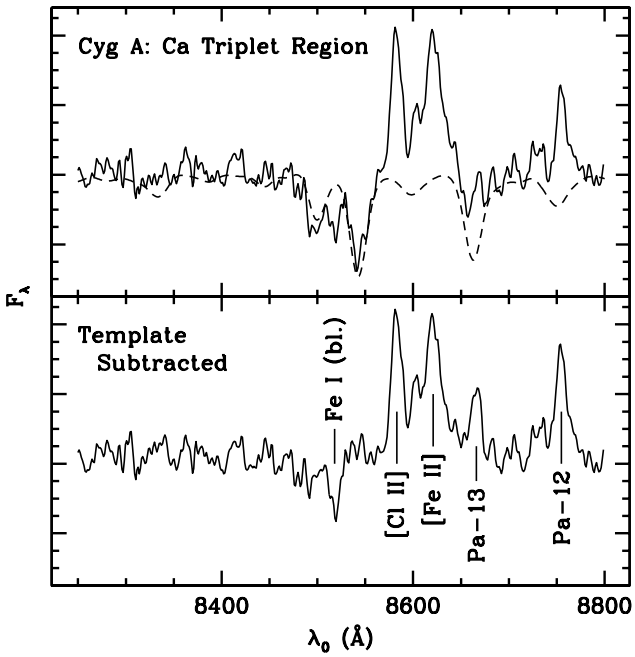

FIG. 4.—*Top*: Spectrum of the Ca triplet region in Cyg A (*solid line*). The continuum has been approximately flattened, and a similarly flattened spectrum of the standard star Wolf 1346 has been smoothed to match the widths of the absorption lines in the Cyg A spectrum (*dashed line*). *Bottom*: Difference between the observed Cyg A spectrum and the Wolf 1346 spectrum.

tion were calculated using redshifts of $z = 0.0562$ for the northwest emission peak and $z = 0.0557$ for the southeast peak, both determined from the prominent Hα and [N II] emission lines in each region. Observed wavelengths of features present in both regions are those of the northwest emission peak. The fluxes were calculated by averaging a five-row block (centered on the row of peak emission, 1 row = 0.″215), and then fitting a Gaussian profile to determine the flux. As can be seen in Figures 2 and 3, the majority of the features are strongest in the northwest emission peak. Of particular interest, though, are those that are evident only in the southeast peak. These three lines are all relatively weak. The two we can identify are [Ar XI] λ6917 and [Fe XI] λ7889 (the latter also seen by O97). High-ionization lines such as these indicate either photoionization by a continuum extending to the far-UV or transient heating by high-speed shocks to $\sim 2 \times 10^6$ K (e.g., Osterbrock & Fulbright 1996). Figure 2 also shows the rise in the nuclear continuum component between the northwest and southeast components toward longer wavelengths.

3.2. *The Calcium Triplet*

Broad absorption from the Ca II triplet lines at 8498, 8542, and 8662 Å cross the central region of Cyg A (see Fig. 2). The detection of these lines gives us the opportunity to check the systemic velocity and estimate the velocity dispersion of the stars in Cyg A.

Initial fits to the calcium triplet lines gave heliocentric redshifts $z = 0.05544$ for the two shorter wavelength lines, but $z = 0.05487$ for the 8662 Å line. From subtraction of a template made by scaling, broadening, and redshifting the calcium triplet lines from the spectrophotometric standard Wolf 1346 (see Fig. 4), it became clear that the longward edge of the λ8662 absorption profile is distorted by an emission line, which we identify as Pa13 (λ8665; this line falls farther to the redward side of the absorption line than one might expect because the emission-line redshift is higher than the absorption-line redshift). We accordingly use only the lines λλ8498, 8542 for estimating the systemic redshift and velocity dispersion. We find $z_{\rm stellar} = 0.05544 \pm 0.0004$ (heliocentric), in satisfactory agreement with the value $z_{\rm stellar} = 0.05562 \pm 0.00015$ found by Stockton, Ridgway, & Lilly (1994) from the λ5184 component of the Mg I *b* feature.

We do not have a suitable template for carrying out a Fourier quotient analysis to estimate the velocity dispersion; instead, we simply estimate the range of broadening of the Ca II λλ8498, 8542 in Wolf 1346 that provides acceptable fits to the features in Cyg A. We find $\sigma = 270 \pm 90$ km s^{-1}, where the large error estimate reflects the low signal-to-noise ratio (S/N) of our continuum spectra in this region. This value is quite consistent with that typically found for central cluster elliptical galaxies.

Terlevich, Díaz, & Terlevich (1990) have used the equivalent width of the Ca triplet lines in active galaxies as a measure of the dilution of the stellar component by featureless continuum components. They found a fairly small dispersion in the equivalent width for a sample, including normal spirals and ellipticals, as well as LINERs and Seyfert galaxies (mostly type 2). Because of contamination from emission and the low S/N of our spectrum, we measured equivalent widths from our Wolf 1346 spectrum after scaling and broadening to give the best fit to the Cyg A spectrum. Using the same measure as Terlevich et al. (1990) (the sum of equivalent widths of the two stronger Ca triplet lines, measured over specific rest-frame bandpasses and corrected for velocity dispersion), we obtain a value of 5.1 Å, which is smaller than the values of all but one of the 42 galaxies in the Terlevich et al. (1990) sample (the equivalent width distribution for their sample has a mean of 7.3 and a standard deviation of 1.0). The smaller value of the equiva-

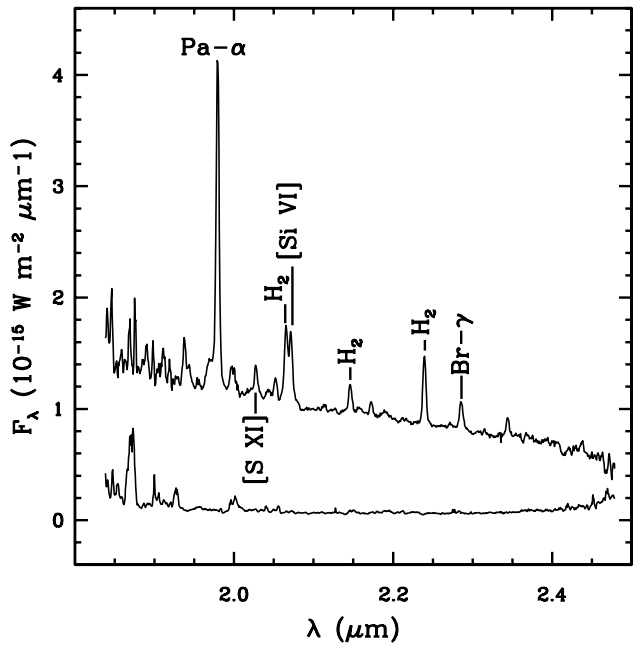

FIG. 5.—Combined near-infrared spectrum of Cygnus A (*upper line*) and 1 σ noise times 5 (*lower line*). The most prominent lines are Paα at 1.979 μm, the blend of H_2 $S(3)$ and [Si VI] at $\sim$2.07 μm, and H_2 $S(1)$ at 2.239 μm (all observed-frame).

lent width in Cyg A indicates that featureless continuum components, which dominate the continuum spectrum in the blue, are still significant at 8500 Å.

3.3. *The IR* 1.9–2.5 μm *Spectrum*

By using a 256 × 256 pixel detector, we have obtained both higher resolution and a significant increase in S/N over the previous study by W91. The spectrum is that of the IR nucleus and is shown in Figure 5. Table 2 lists the major features we have identified. Our measured fluxes are generally a factor of 2 lower than that of W91, probably because of our smaller aperture. The rest wavelengths of the unidentified features were calculated from the average redshift ($z \approx 0.05541$) of the confirmed species. The velocity widths are generally accurate to within $\sim$10%.

TABLE 2

IR EMISSION FEATURES

λ Observed (μm)	λ Rest (μm)	Species[a]	FWHM (km s^{-1})	Flux (W m^{-2})
1.9376	1.8353	H_2 $v = 1$–0 $S(5)$	475	1.87E−18
1.9435	1.8415	?	600	9.83E−19
1.9548	1.8523	H_2 $v = 2$–1 $S(7)$	402	4.50E−19
1.9714[a].....	1.8665	H_2 $v = 6$–4 $O(5)$	?	3.34E−18[b]
1.9714[a].....	1.8721	H_2 $v = 7$–5 $O(3)$	?	...
1.9794	1.8756	Paα	435	1.39E−17
1.9979	1.8914	H_2 $v = 1$–0 $S(4)$	$\lesssim$875[c]	$\lesssim$1.49E−18
2.0274	1.9200	[S XI]	473	1.13E−18
2.0432	1.9359	[Si XI]	$\lesssim$898[c]	$\lesssim$6.21E−19[d]
2.0521	1.9451	Brδ	479	9.79E−19
2.0655	1.9576	H_2 v = 1–0 $S(3)$	582	3.50E−18
2.0713	1.9629	[Si VI]	552	3.03E−18
2.1461	2.0332	H_2 $v = 1$–0 $S(2)$	459	1.21E−18
2.1566	2.0412	H_2 $v = 8$–6 $O(3)$	$\lesssim$746[c]	2.59E−19[d]
2.1724	2.0587	He I	329	5.25E−19
2.1893	2.0729	H_2 $v = 2$–1 $S(3)$	$\lesssim$1351[c]	$\lesssim$6.29E−19
2.2394	2.1218	H_2 $v = 1$–0 $S(1)$	439	3.03E−18
2.2717	2.1536	H_2 $v = 2$–1 $S(2)$	548	$\lesssim$1.99E−19[d]
2.2856	2.1661	Brγ	534	1.30E−18
2.3440	2.2233	H_2 $v = 1$–0 $S(0)$	392	8.13E−19

[a] Approximate central wavelength of unresolved blend.
[b] Total flux of blend.
[c] Probably noise or blend with an unidentified line.
[d] Marginal detection.

4. DISCUSSION

4.1. *High-Ionization Species and Velocity Widths*

We have detected high-ionization species, including [Si VI] 1.962 μm and [S XI] 1.920 μm, which are often considered to be indicators of UV ionization from an active nucleus, although such lines can also be produced in high-speed ($\gtrsim$500 km s^{-1}) shocks (e.g., Dopita & Sutherland 1996). We also have a marginal detection of [Si XI] 1.9359 μm. W91 suggested the possibility that the [Si VI] profile was broader than the H_2 profiles but cautioned that this may be caused by systematic errors. Such a difference in line width could result from some sort of transition between the narrow-line region and BLR. However, we have found no significant difference among the widths of the hydrogen recombination lines, the molecular hydrogen lines, and the high-ionization lines.

It is intriguing that we find strong high-ionization lines both in our IR spectroscopy of the nucleus and our optical spectroscopy of the southeast region, but not in the northwest emission peak. Since we know that scattered radiation from the nucleus is present in the inner region of Cyg A (O97), an attractive possibility is that the extended coronal emission we see near the southeast peak is actually scattered nuclear light. Unfortunately, the S/N of the O97 data for that region is too low to allow the detection of these emission lines in polarized flux.

4.2. *Search for a Broad-Line Region*

Previous spectroscopy of Cyg A has convincingly demonstrated the presence of scattered broad-line radiation (Antonucci et al. 1994; O97). Even if unsuccessful, attempts to detect direct radiation from the BLR in the IR can, in principle, constrain the extinction to the BLR. We discuss here a search for broad Paα, by far the strongest hydrogen recombination line in the near-IR and hence our best opportunity for directly observing the BLR.

Narrow Paα was detected in Cyg A by Lilly & Hill (1987), by W91, and by Stockton & Ridgway (1996). However, our S/N is much higher than that of the first two studies. After correcting for instrument response by assuming a uniformly illuminated slit, we determined the FWHM of Paα to be $\sim$390 km s^{-1}. This is somewhat lower than previous measurements of velocity widths of hydrogen recombination lines: 510 $\pm$ 60 km s^{-1} for Paα (W91) and 500 $\pm$ 100 km s^{-1} for Hβ (Osterbrock & Miller 1975).

Figure 6 is a close-up of the Paα region of the spectrum, showing a blueward bump on the wing of the narrow Paα profile. Initially, we considered the possibility that this could be an offset broad component of Paα. However, we are more likely seeing a blend with the 1.8665 μm $v = 6$–4 $O(5)$ and 1.8721 μm $v = 7$–5 $O(3)$ molecular hydrogen lines seen also by Veilleux, Sanders, & Kim (1997) in their search for hidden BLRs, and there is no clear indication of broad wings to the Paα profile.

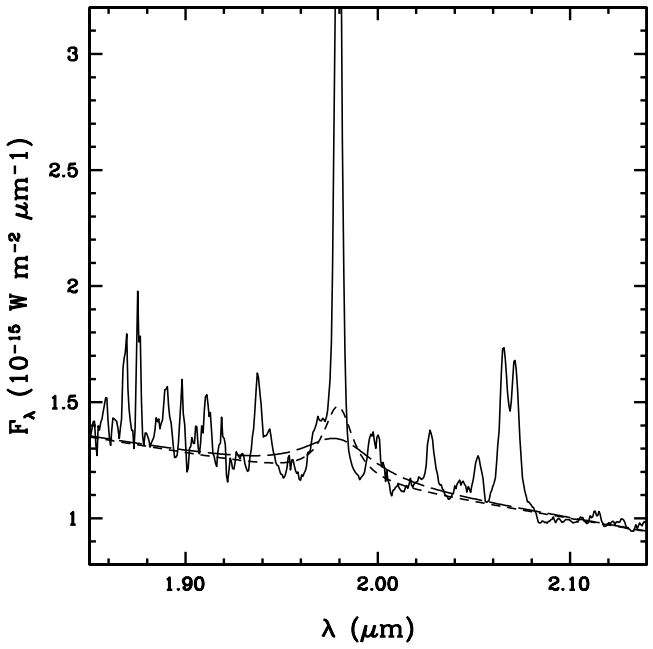

FIG. 6.—Magnified view of the infrared spectrum (*solid line*), showing the strong Paα emission, overplotted with two profiles of widths 3000 km s^{-1} (*short-dashed line*) and 7500 km s^{-1} (*long-dashed line*), representing estimated upper limits to a broad Paα component. The feature immediately blueward of the main profile is likely a blend of two H_2 lines.

In an attempt to estimate the extinction toward the BLR required to conceal any such broad component, we constructed artificial broad Paα profiles to scale against our actual IR spectrum. The results depend critically on the type of profile and width used. In the sample of seven low-redshift quasars studied by Baldwin (1975), the median Hβ FWHM is $\sim$50 Å ($\sim$3000 km s^{-1}), which translates to 190 Å for Paα. The scattered broad lines observed in Cyg A are broader. Antonucci et al. (1994) find an FWHM for [Mg II] of $\sim$7500 km s^{-1}. O97 claim an Hα FWHM 3.5 times as large, or $\sim$26,000 km s^{-1}. From the polarized flux plots of O97 (their Fig. 3*c*–3*d*), we estimate a considerably smaller FWHM of $\sim$15,000 km s^{-1}. It also appears that the profiles have different shapes on the east and west sides of Cyg A, although it is difficult to say how significant this difference is because of contamination by strong narrow emission lines. However, the large difference between the Mg II and Hα profiles and the possible differences between the Hα profile on the two sides introduce a cautionary note regarding whether these scattered components necessarily give the same width that we would find from a direct view of the broad-line region.

Superposed on Figure 6 are two synthetic Paα profiles, having Lorentzian shapes and FWHM of 3000 and 7500 km s^{-1}, corresponding to the median width of Baldwin's sample and the scattered Mg II width found for Cyg A by Antonucci et al. (1994), respectively. It is clear that we cannot place very strong constraints on the presence of profiles significantly broader than the latter.

At the levels we have plotted, which we judge to be close to the limit at which we would just detect it, the broad component of Paα has a flux of $\sim 9.2 \times 10^{-18}$ W m^{-2} for the narrower profile and $\sim 1.1 \times 10^{-17}$ W m^{-2} for the broader one. The difference between these fluxes is much less than the uncertainty in our scaling and too small to significantly affect the estimated extinction, so we have used 10^{-17} W m^{-2} for our calculations.

There are a couple of choices for estimating the intrinsic broad-line flux to use for comparison. Using an empirical relation between X-ray luminosity and broad Hα luminosity in quasars, and assuming the case B ratio between the Hα and Paα broad-line fluxes, W91 derived a predicted broad Paα flux of $\sim 3 \times 10^{-16}$ W m^{-2}. Comparing this with the flux of our artificial broad component to Paα, normalized to the larger aperture of W91 (2.0×10^{-17} W m^{-2}), and correcting for Galactic interstellar extinction, we estimate an extinction (within Cyg A) toward the BLR of $A_V \gtrsim 21$ mag. As an alternative approach, we can use an unobscured quasar apparent magnitude $m_B \approx 14$ (derived from the luminosity estimated by O97). For a mean equivalent width for broad Hβ of $\sim$50 Å (from the composite quasar spectrum of Francis et al. 1991), we calculate $F(\mathrm{H}\beta) \approx 8.3 \times 10^{-16}$ W m^{-2}. Finally, using the case B condition $F(Pa\alpha)/F(\mathrm{H}\beta) \approx 0.3$ (Osterbrock 1989), we arrive at a slightly lower predicted broad Paα flux of $\sim 2.5 \times 10^{-16}$ W m^{-2}, and a corresponding extinction of $A_V \gtrsim 19$ mag. These two extinction estimates are somewhat lower that that of W91 ($A_V \gtrsim 24$ mag), though it is not clear from their paper how they obtained their stated upper limit to a broad component. We feel that our spectrum, with its higher resolution and higher S/N, probably provides a more accurate estimate.

Djorgovski et al. (1991) had suggested that they had detected a quasar nucleus in their K and L' images. However, we are still not seeing any evidence of a BLR at 2 μm, so the object visible in K images is unlikely to be a quasar nucleus. This result is consistent with that of Stockton et al. (1994), who found that the nucleus at K' was not stellar, having a resolved FWHM of $\sim$0.″3.

4.3. *Molecular Hydrogen Emission*

If we interpret the unified model for quasars and radio galaxies in terms of an obscuring molecular torus, significant amounts of molecular gas in these objects should be observed. There are a number of AGN in which near-infrared H_2 emission has been detected, the first being NGC 1068 (Thompson, Lebofsky, & Rieke 1978). The first detection of molecular gas (H_2) in Cygnus A was made by W91. Table 2 lists the large number of molecular hydrogen emission lines we have detected in the infrared.

Some line flux ratios involving H_2 are diagnostics of excitation conditions. One of the most important is the $F[v = 1\text{–}0\ S(3)]/F[v = 1\text{–}0\ S(1)]$ ratio (Kawara, Nishida, & Gregory 1990). This ratio is expected to have a value of about 0.8–1.1 for shock excitation (Kwan 1977; Hollenbach & Shull 1977), 0.5–0.7 for ultraviolet pumping (Sternberg 1988; Black & van Dishoeck 1987), 1.2 for X-ray heating (Lepp & McCray 1983), or 0.6–1.1 for associative detachment and pumping in the transition zone of ionized nebulae (Black, Porter, & Dalgarno 1981). We obtained a ratio of 1.20 ± 0.14. This value would point toward X-ray heating as the most likely excitation mechanism, although shock excitation cannot be excluded by this criterion alone.

Other ratios that can be used for comparison with X-ray heating models are $F[v = 1\text{–}0\ S(1)]/F(\mathrm{Br}\gamma)$ versus $F([\mathrm{O\ I}]\ 6300\ \text{Å})/F(\mathrm{H}\alpha)$. More specifically, Mouri et al. (1989) showed that the H_2 and [O I] emitting regions in their sample of 28 AGN/starburst galaxies are closely related to each other, giving rise to a linear correlation for the above

ratios. Since the [O I] line is in the optical and the H_2 line is in the infrared, the division by the hydrogen recombination line fluxes is done to account for reddening. The values of these ratios we calculated for Cyg A lie essentially on the fit by Mouri et al., which was based on the X-ray heating model by Lepp & McCray (1983) in their sample of 17 Seyfert galaxies (see Fig. 1 in Mouri et al. 1989). This model is characterized by a spherically symmetric cloud of constant gas pressure heated by a central X-ray source.

We were unable to use the traditional 2.248 μm $v = 2$–1 $S(1)$ to $v = 1$–0 $S(1)$ ratio as a diagnostic because the noise in the long wavelengths of our spectrum prevented us from detecting the former line; in any case, this ratio can be misleading (Kawara et al. 1990). However, the two diagnostics that we were able to apply clearly point to X-ray heating from the active nucleus as the most probable excitation mechanism.

5. SUMMARY

There is now considerable evidence that Cygnus A hosts a quasar nucleus, although we believe that it is yet to be observed directly in the optical or IR spectral regions. In particular, we have not managed to achieve a direct detection of broad Paα, in spite of convincing detections of scattered broad Mg II and Hα by Antonucci et al. (1994) and O97, respectively. The line-of-sight extinction must therefore still be very high at 2 μm, our estimate being $\sim$20 mag. However, we have made two important findings. One is the discovery or confirmation of strong high-ionization lines ([Fe XI], [Ar XI], [Si VI], [S XI], and possibly [Si XI]) in both the nucleus and the southeast peak. That the most highly ionized species detected optically, [Fe XI] and [Ar XI], were detected only in the southeast component, while the majority of the emission features were stronger in the northwest emission peak may indicate a scattered nuclear origin for the extended coronal emission lines. Finally, by using the ratios of specific molecular hydrogen transitions we were able to show that X-ray heating is the most likely excitation mechanism for H_2, which again provides important evidence for the role of a quasar-like nucleus in Cygnus A.

We thank Melinda Kellogg for helping with some of the observations, and the referee, Ski Antonucci, for suggesting ways to improve our discussion and presentation. The United Kingdom Infrared Telescope is operated by the Joint Astronomy Centre on behalf of the UK Particle Physics and Astronomy Research Council. The W. M. Keck Observatory is operated as a scientific partnership among the California Institute of Technology, the University of California, and NASA. The Observatory was made possible by the generous financial support of the W. M. Keck Foundation. This project was partially supported by NSF grant AST 95-29078.

REFERENCES

Antonucci, R., Hurt, T., & Kinney, A. 1994, Nature, 371, 313
Baldwin, J. A. 1975, ApJ, 201, 26
Barthel, P. D. 1989, ApJ, 336, 606
Black, J. H., Porter, A., & Dalgarno, A. 1981, ApJ, 249, 138
Black, J. H., & van Dishoeck, E. F. 1987, ApJ, 322, 412
Djorgovski, S., Weir, N., Matthews, K., & Graham, J. R. 1991, ApJ, 372, L67
Dopita, M. A., & Sutherland, R. S. 1996, ApJS, 102, 161
Dressler, A. 1984, ApJ, 286, 97
Francis, P. J., Hewett, P. C., Foltz, C. B., Chaffee, F. H., Weymann, R. J., & Morris, S. L. 1991, ApJ, 373, 465
Hollenbach, D. J., & Shull, J. M. 1977, ApJ, 216, 419
Kawara, K., Nishida, M., & Gregory, B. 1990, ApJ, 352, 433
Kwan, J. 1977, ApJ, 216, 713
Lepp, S., & McCray, R. 1983, ApJ, 269, 560
Lilly, S. J., & Hill, G. J. 1987, ApJ, 315, L103
Mouri, H., Taniguchi, Y., Kawara, K., & Nishida, M. 1989, ApJ, 346, L73
Ogle, P. M., Cohen, M. H., Miller, J. S., Tran, H. D., Fosbury, R. A. E., & Goodrich, R. W. 1997, ApJ, 482, L37 (O97)
Oke, J. B., et al. 1995, PASP, 107, 375
Osterbrock, D. E. 1989, Astrophysics of Gaseous Nebulae and Active Galactic Nuclei (Mill Valley: University Science Books)
Osterbrock, D. E., & Fulbright, J. P. 1996, PASP, 108, 183
Osterbrock, D. E., & Miller, J. S. 1975, ApJ, 197, 535
Pritchet, C. 1978, ApJ, 221, 507
Sternberg, A. 1988, ApJ, 332, 400
Stockton, A., & Ridgway, S. E. 1996, in Cygnus A: Study of a Radio Galaxy, ed. D. Harris & C. Carilli (Cambridge: Cambridge Univ. Press), 1
Stockton, A., Ridgway, S. E., & Lilly, S. J. 1994, AJ, 108, 414
Tadhunter, C. N., Metz, S., & Robinson, A. 1994, MNRAS, 268, 989
Terlevich, E., Díaz, A. I., & Terlevich, R. 1990, MNRAS, 242, 271
Thompson, R. I., Lebofsky, M. J., & Rieke, G. H. 1978, ApJ, 222, L49
Tokunaga, A. 1999, in Astrophysical Quantities, ed. A. N. Cox (New York: AIP), in press
Veilleux, S., Sanders, D. B., & Kim, D.-C. 1997, ApJ, 484, 92
Ward, M. J., Blanco, P. R., Wilson, A. S., & Nishida, M. 1991, ApJ, 382, 115 (W91)